Next Mechanical Engineering 1 (2026) 100004

Contents lists available at ScienceDirect

Next Mechanical Engineering

journal homepage: www.sciencedirect.com/journal/next-mechanical-engineering

A study on combined impact of Cattaneo-Christov heat and mass flux of Casson fluid flow over a curved stretching sheet

Kandavkovi Mallikarjuna Nihaal [a], Shailapura Ramanjineya Pradeepkumar [b], Ulavathi Shettar Mahabaleshwar [b,*], Laura Milena Pérez [c]

[a] Department of Mathematics, Akshaya Institute of Technology, Tumkur 572 106, India
[b] Department of Studies in Mathematics, Davangere University, Shivagangothri, Davangere 577 007, India
[c] Departamento de Ingeniería Industrial y de Sistemas, Universidad de Tarapacá, Casilla 7D, Arica 1000000, Chile

ARTICLE INFO

Keywords:
Casson fluid
Porous medium
Variable thermal conductivity
Melting effect
Curved stretching sheet

ABSTRACT

Non-Newtonian fluid flow across a curved extending surface is significant since it offers a useful insights for various practical applications like polymer sheet extraction, fibre material production, and cooling of curved electronic components. The present study aims to examine the behaviour of Casson fluid over a permeable curved sheet under the influence of variable thermal conductivity and melting effect. Heat and mass transfer over the surface are examined with the aid of Cattaneo-Christov heat flux model. Runge Kutta Felhberg-45th and Shooting approach is used to gain a numerical solution for this fluid model. Then those numerical outcomes are examined visually through graphs. The main outcomes reveal that fluid flow slows down for rising values of the porosity parameter but increases for the curvature parameter. Whereas, the thermal profile elevates for larger values of variable thermal conductivity but declines for thermal relaxation parameter. Both curvature and concentration relaxation parameters reduce concentration gradients across the surface. In addition, the heat and mass transfer rates are reduced for curvature parameter, and thermal and concentration relaxation parameters respectively. In addition, the work discusses the behaviour of engineering factors against certain influencing parameters. The results of present study simulates a non-Newtonian fluid flow with melting effect offers significant insights which can be applicable on metal casting, and regulating heat management in curved electronics.

1. Introduction

Casson fluid, a non-Newtonian fluid system, behaves as a solid unless a specific limit is crossed, then it behaves as a fluid and starts to flow. These kinds of non-Newtonian fluids have a distinct yield stress and varied viscosity, unlike other Newtonian fluid models. The Casson fluid model possesses a characteristic shear thinning properties that simulates fluid flow behaviour in bio-logical and industrial fluids. This model is useful in circumstances like heat exchange systems, biomedical systems, and food processing industries, where the Newtonian fluid model fails. The Casson parameter indicates the proportion between yield stress and plastic dynamic viscosity, where a larger Casson parameter suggests weaker yield stress effects and exhibits flow behaviour approaching the Newtonian limit. Kumar et al. [1] examined the Casson fluid's nature across a curved sheet with exponential stretching under the impact of Magneto Hydro Dynamics (MHD) and thermal radiation. The study results revealed that the momentum profile declines for increasing Casson parametric values. Awais et al. [2] explored the effects of joule heating and MHD on Darcy Forchhiemer imposed Casson nanofluid flow over oscillating vertical surface. The results show that fluid velocity slows down for growing value of Casson parameter. Considering Casson fluid model, Jat et al. [3] analyzed the impacts of joule heating, thermophoresis and Brownian motion on Darcy Forchhiemer fluid flow past a bended stretching surface. The results show that growing values of Casson parameter rises fluid flow. Saleem et al. [4] investigated the behaviour of Cason nanofluid flow across a porous curved surface under the influence of radiation, viscous dissipation, and entropy generation. The influence of heat source/sink over MHD Casson nanofluid flow was studied by Nihaal et al. [5]. The study results reveal that momentum profile hinder for growing values of Casson parameter.

Porous medium is critical for fluid behaviour due to its flow-changing property when compared with free-flow. Fluids in this condition encounter frictional resistance and low velocities as they pass

* Corresponding author.
E-mail address: u.s.m@davangereuniversity.ac.in (U.S. Mahabaleshwar).

https://doi.org/10.1016/j.nxmech.2026.100004
Received 28 September 2026; Received in revised form 8 November 2026; Accepted 11 November 2026
Available online 12 November 2026
3117-9258/© 2026 Published by Elsevier Ltd. This is an open access article under the CC BY-NC-ND license (http://creativecommons.org/licenses/by-nc-nd/4.0/).

Nomenclature

a	Constant
C_s	Specific heat capacity of solid surface $(m^2s^{-2}K^{-1})$
Cp	Specific heat capacity of fluid $(m^2s^{-2}K^{-1})$
C_w	Concentration at surface (kgm^{-3})
C_m	Concentration at melting surface (kgm^{-3})
C_∞	Concentration at far field (kgm^{-3})
C_f	Skin friction
D_B	Diffusivity (m^2s^{-1})
K	Permeability (m^2)
K_T	Variable thermal conductivity $(kgms^{-3}K^{-1})$
K_∞	Far field thermal conductivity $(kgms^{-3}K^{-1})$
Me	Melting parameter
Pr	Prandtl number
R	Radius of curved surface (m)
Re_s	Reynolds number
$(r,\ s)$	Cylindrical coordinates (m)
Sc	Schmidt number
Sh	Sherwood number
T_0	Constant temperature of solid medium (K)
T_m	Temperature of melting surface (K)
T_∞	Far field temperature (K)
u_w	Surface velocity (ms^{-1})
q_s	Wall heat flux
q_c	Wall mass flux

Symbols

α	Porosity parameter
υ	Kinematic viscosity (m^2s^{-1})
ρ	Density (kgm^{-3})
β	Casson fluid parameter
δ	Fluid's latent heat
λ_1	Thermal relaxation parameter
ζ_1	Concentration relaxation parameter
$\in$	Thermal conductivity parameter
τ_{rs}	Wall shear stress $(kgm^{-1}s^{-2})$
Θ	Curvature parameter

Subscripts

f	Base fluid

Abbreviations

MHD	Magneto Hydro Dynamics
C-C	Cattaneo-Christov
PDEs	Partial Differential Equations
ODEs	Ordinary Differential Equations
BVP	Boundary Value Problem
IVP	Initial Value Problem
RKF	Runge Kutta Fehlberg

through this medium. Boundary layer flow depends upon the porous medium to manage thermal fluid correlations, as it affects heat and mass transfer rates in fluid flow. It has many applications, such as in biochemical industries, energy exchange systems, and gas and oil extractions. Ahmad et al. [6] investigated fluid flow across a porous stretched surface in the presence MHD. The findings show that as the porosity parameter and MHD is raised, the drag force enhances. Mumtaz et al. [7] explored the behaviour of gyrostatic microorganisms in ternary nanofluid flow over curved porous stretching sheet under the effects of radiation. It is discovered that as the porosity is raised, the fluid profile falls. Ahsan et al. [8] examined the effects of a chemical reaction phenomenon on second grade MHD fluid flow over curved stretching sheet with Darcy-Forchheimer model. Richa et al. [9] studied the outcomes of ANN and entropy formation in a formulation in a nanofluid flow that passed through a curved stretched surface due to MHD. Observations show that momentum and thermal field both increase with increasing values of Forchheimer porosity parameter. Numerical work on the Williamson fluid flow over a porous curved stretching sheet in the presence of chemical reaction and microbes was carried out by Ahsan et al. [10]. It is evident that the fluid velocity profile dropped due to increasing porosity parameter.

Variable thermal conductivity is defined as a thermal conductivity of the fluid that varies with temperature, pressure, or concentration. Classical heat transfer models often consider a constant conductivity for fluid materials, but in reality, conductivity may vary with temperature changes. The relevance of changing thermal conductivity in the temperature field is that it alters the distribution of heat within the medium. This effect is often represented in a temperature equation of the mathematical model as a function of temperature. Murtaza et al. [11] investigated the impacts of varying thermal conductivity on thermal transfer across a curved extending sheet in the presence of MHD. The findings demonstrate that increasing values of variable thermal conductivity promotes fluid flow and overall temperature of the fluid. Awais et al. [12] explored magnetic field imposed Eyring powell fluid flow between parallel plates under the influence of variable thermal conductivity and activation energy. Ahmed et al. [13] scrutinised the effects of activation energy and variable thermal conductivity on Williamson fluid flowing over a non-linear extended curved sheet. The influence of variable thermal conductivity over different fluid model and geometries can be found in these works [14,15].

When a heated fluid starts to transmit heat to the solid surface that is in contact with it, this phenomenon is referred to as the melting effect at the boundary surface. Modern innovative thermal engineering has found significant uses for the melting effect in non-Newtonian fluid flows, such as welding, geothermal energy extraction, preservation of latent heat, and many more. Roberts pioneered studying the melting effect in this boundary layer flow field [16]. Followed by Robert, the influence of the melting effect was analysed by Tien and Ten [17] for heat transfer over forced convective flow. Obalalu et al. [18] examined the impact of the melting effect on a Casson-based Williamson non-Newtonian fluid under the influence of hetero/homogeneous chemical reactions. Recently, the distinct fluid models over a curved stretching sheet are studied by many researchers [19,20].

A curved stretching sheet is a dynamically deforming, non-flat surface that is being stretched in its own plane, the surface is curved, not flat. The flow and heat transfer characteristics are affected by the curvature, which adds further geometric effects to the boundary layer equations in these types of problems. In this field of research, the traditional flat stretching sheet model is expanded to include more realistic shapes that are found in the manufacturing industries. These studies [21,22] show the applicability of Mechanics-based neural network and Physics informed neural network prediction has been incorporated to analyse heat and mass transfer across curved surface. Nadeem et al. [23] examined the effect of variable viscosity on MHD nanofluid flow. The results show that fluid velocity rises and temperature lowers for increasing values of the curvature parameter.

Ragupathi et al. [24] studied the influence of gyrotactic microorganisms on MHD nanofluid flow in the presence of Thermophoresis and Brownian motion. The study reveals that motile density reduces for larger values of the curvature parameter. Nagaraja et al. [25] investigated chemically reactive ternary nanofluid flow across a bended porous extending sheet under the impact of C-C heat flux numerically.

Aldandani and Jan [26] investigated non-non-similar solution for Reiner Philippoff fluid flow across a curved sheet due to the effect of thermal radiation. Sharma and Sharma [27] employed response surface methodology to carry out statistical analysis on nanofluid flow over a nonlinear curved surface with a magnetic field and heat source sink effects.

Based on the studies mentioned earlier, it is clear that no research has been conducted on the mixed impacts of porous medium, variable thermal conductivity, melting effect, and C-C heat flux model over non-Newtonian fluid flow across a curved stretching sheet model. Hence, the primary objective of the current study is to address the aforementioned gap. As a result, the current work derives the applicable PDEs for our model with appropriate similarity variables and obtains numerical solutions for the resulting non-linear ODEs. The results from the present study can give significant insights into improving industrial processes such as metal coatings, polymer sheet extrusion, energy exchangers, and biomedical applications, like drug delivery studies in curved arteries. Table 1 demonstrates the significant novelty of the present work in comparison with already published works.

2. Mathematical modelling

The present model has considered a two dimensional, steady and incompressible non-Newtonian fluid model over a curved extended porous surface formed circularly with a radius of R. Therefore, the model is curved stretching sheet with cylindrical coordinates (r, s), where r denotes the radial distance measured normal to the surface and s indicates tangential coordinates measured along the curved surface. The surface of the sheet is deformed around a semicircle of radius R under the impact of two equally opposing forces in the s direction, with the origin held stationary and its velocity $u_w(s) = as$ along s direction, where a indicates the stretching constant (see Fig. 1). Further, heat and mass transfer are analysed under the influence of variable thickness and C-C heat flux and mass flux. The temperature of the surface melting and at the far field are denoted by (T_m, T_∞) where $T_m < T_\infty$ and T_0 the constant temperature of the solid medium satisfies $T_m > T_0$. Also, rheological equation of state for an Casson nanofluid is given as,

$$\widehat{\tau}_{ij} = \begin{cases} 2e_{ij}\left[p_y \Big/ (2\pi)^{0.5} + \mu_b\right] : \pi_c < \pi \\ 2e_{ij}\left[p_y \Big/ (2\pi_c)^{0.5} + \mu_b\right] : \pi_c > \pi \end{cases},$$

Here, $\widehat{\tau}_{ij}$ is the Cauchy stress tensor along $(i, j)^{th}$ component, π are multiple of deformation rate constant with itself and π_c is the critical value of this multiple based on non-Newtonian fluid model, μ_b denotes plastic dynamic viscosity and p_y is the yield stress of the non-Newtonian fluid. Based on the above considerations, the velocity, thermal, and concentration equations are derived as follows (see [11,20,28,29]):

$$\frac{\partial}{\partial r}[(r+R)v] + R\frac{\partial u}{\partial s} = 0, \tag{1}$$

Table 1
Comparison of current work with earlier published works.

Works	[11]	[20]	[4]	[28]	Current work
Casson	×	×	✓	×	✓
Porous medium	×	✓	×	×	✓
Variable thermal conductivity	✓	×	×	×	✓
C-C heat and mass flux	×	×	×	✓	✓
Melting effect	×	✓	×	×	✓
Curved geometry	✓	✓	✓	✓	✓
Fluid category					
Mono	×	✓	×	×	×
Hybrid	×	×	×	✓	×
Ternary	×	×	×	×	×

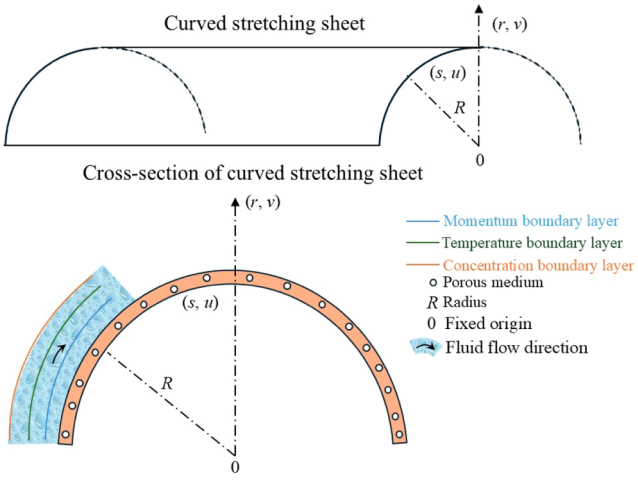


Fig. 1. Schematic diagram of the flow model.

$$\frac{1}{R+r}u^2 = \frac{1}{\rho_f}\frac{\partial p}{\partial r}, \tag{2}$$

$$\begin{aligned} &\frac{uv}{r+R} + u\frac{\partial u}{\partial s}\left(\frac{R}{r+R}\right) + v\frac{\partial u}{\partial r} = -\left(\frac{1}{\rho_f}\left(\frac{R}{r+R}\right)\frac{\partial p}{\partial s}\right) \\ &+\upsilon_f\left(1+\frac{1}{\beta}\right)\left[\frac{\partial^2 u}{\partial r^2} + \frac{1}{r+R}\frac{\partial u}{\partial r} - \frac{u}{(r+R)^2}\right] - \frac{\upsilon_f}{K}u \end{aligned}, \tag{3}$$

$$\begin{aligned} &u\frac{\partial T}{\partial s}\left(\frac{R}{r+R}\right) + v\frac{\partial T}{\partial r} = \frac{1}{\rho_f Cp_f}\left(\frac{1}{r+R}\right)\frac{\partial}{\partial r}\left[(r+R)K_T\frac{\partial T}{\partial r}\right] \\ &-\lambda\left[\begin{array}{l} \frac{\partial^2 T}{\partial s^2}u^2\left(\frac{R}{r+R}\right)^2 + 2\left(\frac{R}{r+R}\right)uv\frac{\partial^2 T}{\partial r\partial s} + \frac{\partial^2 T}{\partial r^2}v^2 \\ +\frac{\partial T}{\partial s}\left(\left(\frac{R}{r+R}\right)v\frac{\partial u}{\partial r} + u\left(\frac{R}{r+R}\right)^2\frac{\partial u}{\partial s}\right) \\ +\frac{\partial T}{\partial r}\left(v\frac{\partial v}{\partial r} + \left(\frac{R}{r+R}\right)u\frac{\partial v}{\partial s}\right) \end{array}\right] \end{aligned}, \tag{4}$$

$$\begin{aligned} &u\frac{\partial C}{\partial s}\left(\frac{R}{r+R}\right) + v\frac{\partial C}{\partial r} = D_B\left[\frac{\partial^2 C}{\partial r^2} + \frac{\partial C}{\partial r}\left(\frac{1}{r+R}\right)\right] \\ &-\zeta\left[\begin{array}{l} \frac{\partial^2 C}{\partial s^2}u^2\left(\frac{R}{r+R}\right)^2 + \frac{\partial^2 C}{\partial r^2}v^2 + 2uv\left(\frac{R}{r+R}\right)\frac{\partial^2 C}{\partial r\partial s} \\ +\frac{\partial C}{\partial s}\left(\left(\frac{R}{r+R}\right)v\frac{\partial u}{\partial r} + u\left(\frac{R}{r+R}\right)^2\frac{\partial u}{\partial s}\right) \\ +\frac{\partial C}{\partial r}\left(v\frac{\partial v}{\partial r} + \left(\frac{R}{r+R}\right)u\frac{\partial v}{\partial s}\right) \end{array}\right] \end{aligned}, \tag{5}$$

Boundary conditions are

$$\begin{aligned} &\text{at} r = 0 : u = u_w, \quad K_T\left(\frac{\partial T}{\partial r}\right)_{r=0} = \rho_f[\delta + C_s(T_w - T_o)]v(s,0), \quad T \\ &= T_m, \quad C = C_m, \end{aligned} \tag{6}$$

$$\text{as} r \to \infty : u \to 0, \quad \frac{\partial u}{\partial r} \to 0, T \to T_\infty, \quad C \to C_\infty \tag{7}$$

Here, velocities (u, v) are along coordinates (s, r). υ_f denotes kinematic viscosity, $\left(Cp_f, \rho_f\right)$ are the specific heat capacity and density of the fluid, $\beta = \mu_b\sqrt{2\pi_c}/p_y$ denotes Casson fluid parameter, K is the permeability, (λ, ζ) are thermal relaxation and concentration relaxation parameters, D_B denotes diffusivity, (δ, C_s) are the fluid's latent heat and the specific heat capacity of the solid surface, (C_m, C_∞) are

concentration of the fluid at the melting surface and at the far field respectively.

The variable thermal conductivity (K_T) in the Eq. (4) is a function of temperature and is defined as follows (see [11]):

$$K_T = K_\infty(1 + \in \theta(\eta)) \tag{8}$$

Where, $\in$ indicates the thermal conductivity parameter, and K_∞ indicates the far-field thermal conductivity of the fluid from the surface.

The following similarity variables are used for transformation,

$$u = asf'(\eta),\ v = -\left(\frac{R}{r+R}\right)(av_f)^{1/2}f(\eta),\ \eta = r\left(\frac{a}{v_f}\right)^{1/2} \tag{9}$$

$$p = \rho_f a^2 s^2 P(\eta),\ \theta(\eta) = \frac{T - T_m}{T_\infty - T_m},\ \chi(\eta) = \frac{C - C_w}{C_w - C_\infty} \tag{10}$$

Using similarities (9) and (10), the equations from (1) to (7) take reduced form as follows:

$$\frac{\partial P}{\partial \eta} = \frac{f^2(\eta)}{\eta + \Theta}, \tag{11}$$

$$\begin{aligned}&\left(1+\frac{1}{\beta}\right)\left[f^{iv}(\eta) + \frac{2f'''(\eta)}{(\eta+\Theta)} - \frac{f''(\eta)}{(\eta+\Theta)^2} + \frac{f'(\eta)}{(\eta+\Theta)^3}\right]\\ &+\frac{\Theta}{(\eta+\Theta)}\left(f'''(\eta)f(\eta) - f''(\eta)f'(\eta)\right) + \frac{\Theta}{(\eta+\Theta)^2}\left(f''(\eta)f(\eta) - f'^2(\eta)\right),\\ &-\frac{\Theta}{(\eta+\Theta)^3}f''(\eta)f(\eta) - \alpha\left(\frac{f'(\eta)}{(\eta+\Theta)} + f''(\eta)\right) = 0\end{aligned} \tag{12}$$

$$\begin{aligned}&\frac{1}{\mathrm{Pr}}\left[\theta''(\eta)(1+\in\theta(\eta)) + \frac{1}{(\eta+\Theta)}\theta'(\eta)(1+\in\theta(\eta)) + \in\theta'^2(\eta)\right]\\ &+f(\eta)\theta'(\eta)\frac{\Theta}{(\eta+\Theta)} - \lambda_1\left[\left(\frac{\Theta}{\eta+\Theta}\right)^2\begin{pmatrix}\theta''(\eta)f^2(\eta) + \theta'(\eta)f(\eta)f'(\eta)\\ -\frac{1}{(\eta+\Theta)}\theta'(\eta)f^2(\eta)\end{pmatrix}\right] = 0\end{aligned}, \tag{13}$$

$$\begin{aligned}&\frac{1}{Sc}\left[\chi''(\eta) + \frac{\chi'(\eta)}{(\eta+\Theta)}\right] + \frac{\Theta}{(\eta+\Theta)}f(\eta)\chi'(\eta)\\ &-\zeta_1\left[\left(\frac{\Theta}{\eta+\Theta}\right)^2\begin{pmatrix}f^2(\eta)\chi''(\eta) + f(\eta)f'(\eta)\chi'(\eta)\\ -\frac{1}{(\eta+\Theta)}f^2(\eta)\chi'(\eta)\end{pmatrix}\right] = 0\end{aligned}. \tag{14}$$

with the modified boundary conditions,

$$f'(0) = 1,\quad Me\theta'(0) + \mathrm{Pr}f(0) = 0, \theta(0) = 0,\quad \chi(0) = 0, \tag{15}$$

$$f'(\infty)\to 0, f''(\infty)\to 0, \theta(\infty)\to 1\theta(\infty)\to 1,\quad \chi(\infty)\to 1 \tag{16}$$

where, ($\lambda_1 = a\lambda, \zeta_1 = a\zeta$), $\Theta = \sqrt{\frac{a}{v_f}}R$, $\alpha = \frac{v_f}{Ka}$, $\mathrm{Pr} = \frac{(\rho Cp)_f v_f}{K_\infty}$, $Sc = \frac{v_f}{D_B}$, $Me = \frac{Cp_f(T_\infty - T_m)}{\delta + C_s(T_m - T_0)}$ are thermal and concentration relaxation parameters of C-C heat and mass flux model, curvature parameter, porosity parameter, Prandtl number, Schmidt number, and melting parameter.

The resultant engineering coefficients with their reduced form are as follows:

Skin friction: $Cf_s = \left(1 + \frac{1}{\beta}\right)\frac{\tau_{rs}}{\rho_f u_w^2}$, where $\tau_{rs} = \mu\left(\frac{\partial u}{\partial r} - \frac{u}{r+R}\right)\Big|_{r=0}$.

$$\Rightarrow Cf_s\mathrm{Re}_s^{1/2} = \left(f''(0) - \frac{f'(0)}{\Theta}\right)\left(1 + \frac{1}{\beta}\right). \tag{17}$$

Nusselt number: $Nu_s = \frac{sq_s}{K_T\Delta T}$, where $q_s = K_T\frac{\partial T}{\partial r}\Big|_{r=0}$

$$\Rightarrow Nu_s\mathrm{Re}_s^{-1/2} = -\theta'(0). \tag{18}$$

Sherwood number: $Sh_s = \frac{sq_c}{\Delta C}$, where $q_c = D_B\frac{\partial C}{\partial r}\Big|_{r=0}$

$$\Rightarrow Sh_s\mathrm{Re}_s^{-1/2} = -\chi'(0) \tag{19}$$

3. Numerical methodology

The reduced Eqs. (12–14) and boundary conditions (15−16) are a higher order Boundary Value Problem (BVP) and have to convert to Initial Value Problem (IVP). Hence, the numerical solution is obtained by RKF-45th and the Shooting method. In this combined procedure, initially, new parameters are introduced to reduce the highly ordered nonlinear ODEs to a system of 1st order equations. This procedure is given as follows:

$$f = y_1,$$

$$f' = y_2,$$

$$f'' = y_3,$$

$$f''' = y_4,$$

$$\begin{aligned}y_4' = &-\left(\frac{1}{\left(1+\frac{1}{\beta}\right)}\right)\left(\begin{array}{l}\frac{\Theta}{(\eta+\Theta)}(y_1y_4 - y_2y_3)\\ +\frac{\Theta}{(\eta+\Theta)^2}(y_1y_3 - y_2^2)\\ -\frac{\Theta}{(\eta+\Theta)^3}y_1y_3 - \alpha\left(\frac{y_2}{(\eta+\Theta)} + y_3\right)\end{array}\right)\\ &-\left[\frac{2y_4}{(\eta+\Theta)} - \frac{y_3}{(\eta+\Theta)^2} + \frac{y_2}{(\eta+\Theta)^3}\right]\end{aligned} \tag{20}$$

$$\theta = y_5,$$

$$\theta' = y_6,$$

$$y_6' = -\left(\frac{1}{\left\{\frac{(1+\in y_5)}{\mathrm{Pr}} - \lambda_1\left(\frac{\Theta}{\eta+\Theta}\right)^2 y_1^2\right\}}\right)\left(\begin{array}{l}\frac{1}{\mathrm{Pr}}\left[(1+\in y_5)\frac{y_6}{(\eta+\Theta)} + \in y_6^2\right]\\ +\left\{\frac{\Theta}{\eta+\Theta}\right\}y_1y_6\\ -\lambda_1\left\{\frac{\Theta}{\eta+\Theta}\right\}^2\left\{\begin{array}{l}y_1y_2y_6\\ -\frac{1}{(\eta+\Theta)}y_1^2y_6\end{array}\right\}\end{array}\right), \tag{21}$$

$$\chi = y_7,$$

$$\chi' = y_8,$$

$$y_8' = -\left(\frac{1}{\left\{\frac{1}{Sc} - \zeta_1\left(\frac{\Theta}{\eta+\Theta}\right)^2 y_1^2\right\}}\right)\left(\begin{array}{l}\frac{1}{Sc}\left\{\frac{y_8}{(\eta+\Theta)}\right\} + \left\{\frac{\Theta}{\eta+\Theta}\right\}y_1y_8\\ -\zeta_1\left\{\frac{\Theta}{\eta+\Theta}\right\}^2\left\{\begin{array}{l}y_1y_2y_8\\ -\frac{1}{(\eta+\Theta)}y_1^2y_8\end{array}\right\}\end{array}\right). \tag{22}$$

and

$$y_2(0) = 1,\quad y_5(0) = 0,\quad Mey_6(0) + Pry_1(0) = 0,\quad y_7(0) = 0 \tag{23}$$

$$y_2(\infty)\to 0, y_3(\infty)\to 0, y_5(\infty) = 0,\quad y_7(\infty) = 1 \tag{24}$$

The solution procedure is as follows: Initially, the shooting method assumes unknown initial values to convert the BVP into an IVP. These values are altered until boundary constraints are satisfied at the far end.

In addition, iteration ends when there is no longer a significant difference between current and earlier repetitive values of momentum, thermal, and concentration profiles. The convergence threshold is set at 0.0001 to get precise numerical findings. Next, the obtained IVP is solved with the help of the RKF-45th method. During the simulation, the step size is assumed to be $h = 0.01$. The validation of the present work with published work is displayed in Table 2. The good matching between previous work and current work shows the numerical method's precision and stability.

4. Results and discussion

The present part addresses the computational findings of Casson fluid flow along a permeable curved stretching sheet in the presence of variable thermal conductivity, C-C heat and mass flux model, and melting effect. The following are the default parameter values chosen during simulation. $\beta = 0.5$, $\Theta = 0.5$, $\alpha = 0.6$, $\lambda_1 = 0.5$, $M_E = 1.1$, $\zeta_1 = 0.5$, and $\in = 0.6$. The simulation is carried out in two cases: i) when $\beta = 0.5$, which denotes a non-Newtonian fluid behaviour, and ii) $\beta \to \infty$ which denotes that the fluid behaves as a Newtonian fluid.

Fig. 2 shows the behaviour of the velocity profile $f'(\eta)$ for several values of Casson parameter β over. From the figure, it is observed that $f'(\eta)$ drops for increasing β values. Physically, the growing values of β, increases effective viscosity which in turn slows down velocity transfer. Hence, the velocity boundary layer experiences resistance to deformation causing reduction in fluid flow.

The effect of the curvature parameter Θ on $f'(\eta)$ is depicted in Fig. 3. A rise in $f'(\eta)$ is observed for augmented values of Θ. Physically, as the curvature parameter is raised, it results in a higher radius of curvature, which in turn facilitates faster and more seamless fluid flow over the surface. As a consequence, the fluid experiences greater momentum transfer over the surface. Further, it is found that the effect is more pronounced for non-Newtonian case in relative with Newtonian case. This is because the viscosity of Casson fluid, decreases as the shear stress increases, and the local shear stress close to the curved surface elevates for a growing curvature, resulting in lower viscosity, thus increasing fluid velocity.

Fig. 4 displays the increment in $f'(\eta)$ for varying values of the porosity parameter α. Physically, when porosity parameter is increased, the cross-sectional area reduces, lowering permeability. The resulting permeability decreases fluid flow velocity. Further, compared to non-Newtonian fluids, the reduction is greater in the Newtonian case. This is because viscosity is constant in Newtonian fluids, and in addition to the resistive drag force by porous material, it leads to an immediate fall in flow velocity.

Curvature parameter Θ influence over $\theta(\eta)$ is shown in Fig. 5. From figure is clear that $\theta(\eta)$ increases for varying larger values of Θ. Physically, as the curvature increases, the thickness of thermal boundary layer gets increases and hence temperature profile rises for increasing curvature parameter. Further, the raise in $\theta(\eta)$ is seen more pronounced for the Newtonian case compared to non-Newtonian case.

The impact of λ_1 over thermal profile $\theta(\eta)$ is shown in Fig. 6. It is clear from the figure that $\theta(\eta)$ decreases for rising values of λ_1. From physical point of view, as the thermal relaxation parameter is elevated it slows down heat transfer. Moreover, compared to the Newtonian case, the reduction is observed to be stronger for the non-Newtonian case because of its rheological behaviour and low heat diffusion capabilities.

Table 2
Validation of numerical results of skin friction with existing work.

Curvature parameter Θ	[20]	Present study
5	0.75763	0.75761
10	0.87349	0.87345
20	0.93561	0.93559
30	0.95686	0.95684
40	0.96759	0.96753
50	0.97405	0.97402

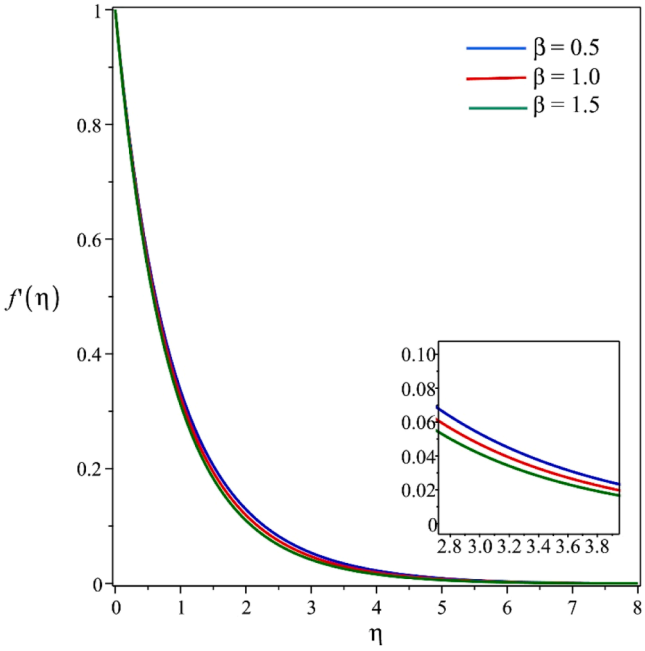


Fig. 2. Variation of $f'(\eta)$ for different β values.

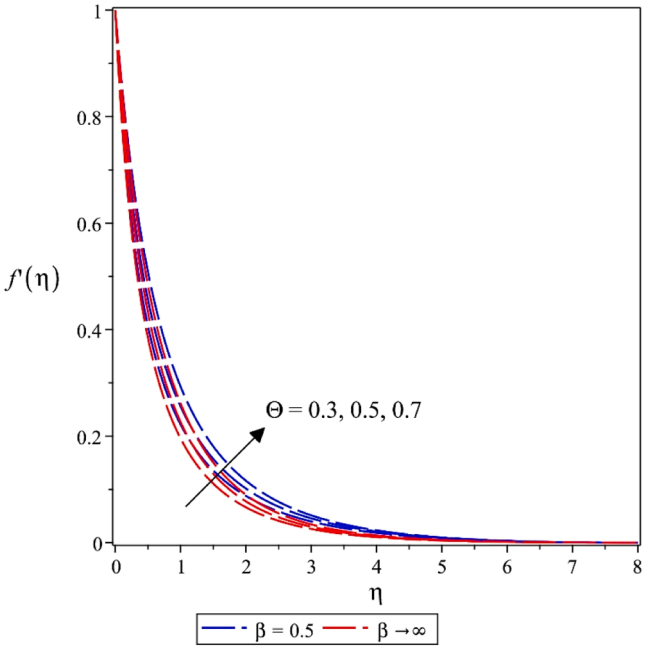


Fig. 3. Influence of Θ on $f'(\eta)$.

The influence of $\in$ over $\theta(\eta)$ is observed in Fig. 7. The plot shows that $\theta(\eta)$ rises for growing values of $\in$. Physically, with an increment in this parameter, the heat transfer from the surface to the fluid becomes more effective due to temperature dependent thermal conductivity. The raise is more pronounced in the Newtonian case because of the absence of yield stress effect which allows smoother flow and stronger heat transport.

The impact of M_E over $\theta(\eta)$ is shown in Fig. 8. It is observed that the thermal profile declines as M_E increases. Physically, the melting effect acts as a blowing boundary condition, which, supresses heat transfer from the wall, thereby reducing thermal boundary thickness. This

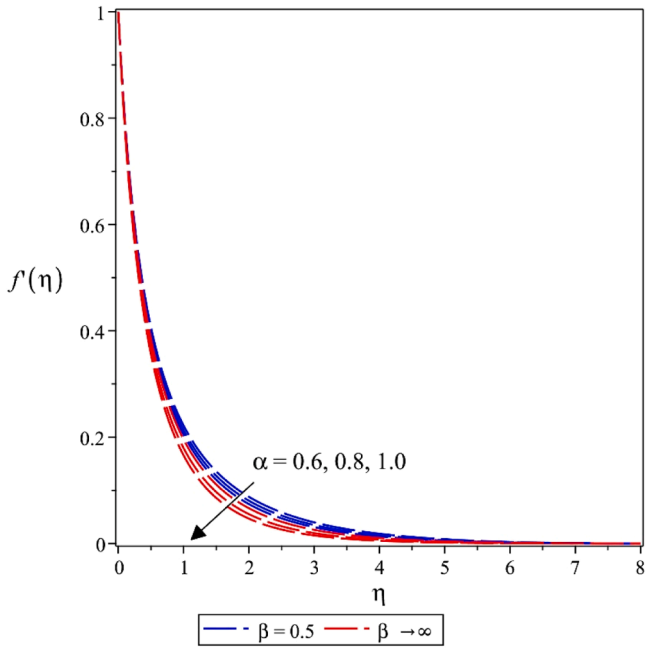


Fig. 4. Influence of α on $f'(\eta)$.

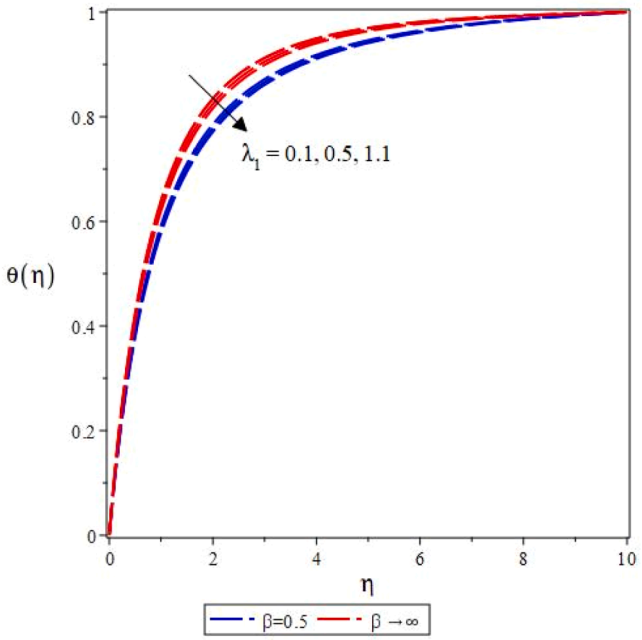


Fig. 6. Impact of λ_1 impact on $\theta(\eta)$.

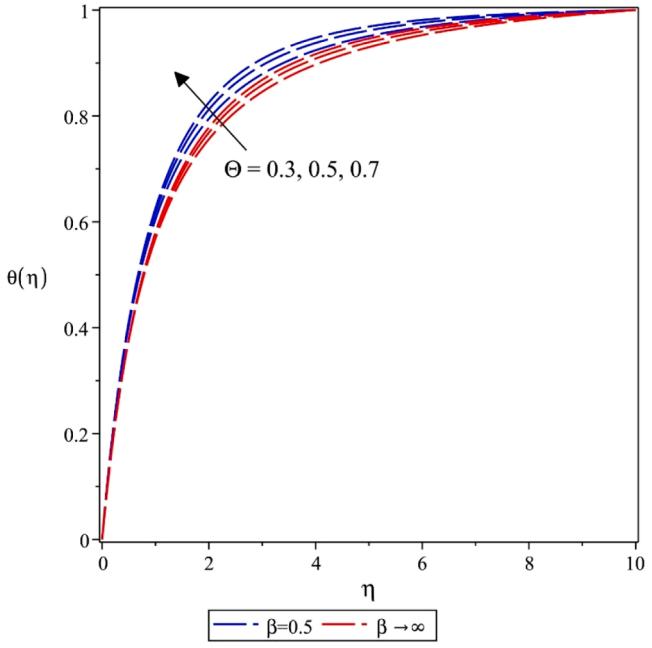


Fig. 5. Influence of Θ on $\theta(\eta)$.

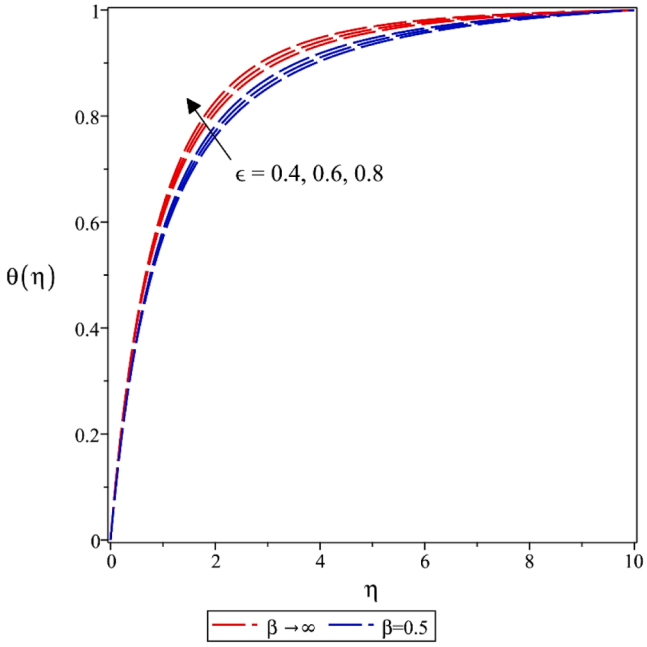


Fig. 7. Impact of $\in$ over $\theta(\eta)$.

reduces the overall temperature of the fluid. Due to constant viscosity, the Newtonian case exhibits more decrease in temperature profile compared to the non-Newtonian case.

The effect of curvature parameter Θ over $\chi(\eta)$ is displayed in Fig. 9. From the figure, the rise in $\chi(\eta)$ is observed for varying values of Θ. Physically, a rise in curvature parameter leads to a flat surface which increases convection and expanding leading to thickening of concentration boundary layer. As a result, the concentration profile increases for growing values of curvature. Further it is seen that the increment is seen more in Newtonian case compared to non-Newtonian case.

Fig. 10 demonstrates the effect of ζ_1 over $\chi(\eta)$. The plot explains the increment in $\chi(\eta)$ for growing values of ζ_1. Physically, the growing values of the relaxation parameter in a curved stretching sheet lead to a reduction in amount of diffusive transport, while the curvature induced decrease in effective stretching slows down convective diffusion. As a consequence, species aggregate toward the surface, causing the concentration profile to elevate. The increment is larger in Newtonian case when compared with non-Newtonian case.

The variation in Skin friction Cf_s for growing values of β and Θ are demonstrated in Fig. 11. As shown in the figure, Cf_s shows an increasing trend for rising values of Θ and a decreasing trend for rising values of β. Physically, when a curved surface is stretched, it exerts additional shear stress on the fluid flow, which elevates the skin friction factor, and in parallel, the curves are dropped due to the strong viscosity when the Casson parameter is elevated.

The variation in the Nusselt number Nu_s for λ_1 and Θ are displayed in

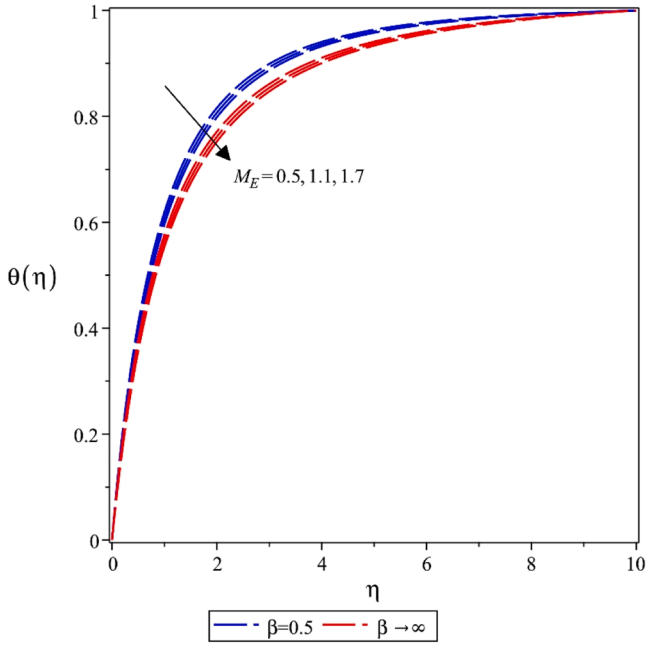


Fig. 8. Impact of M_E over $\theta(\eta)$.

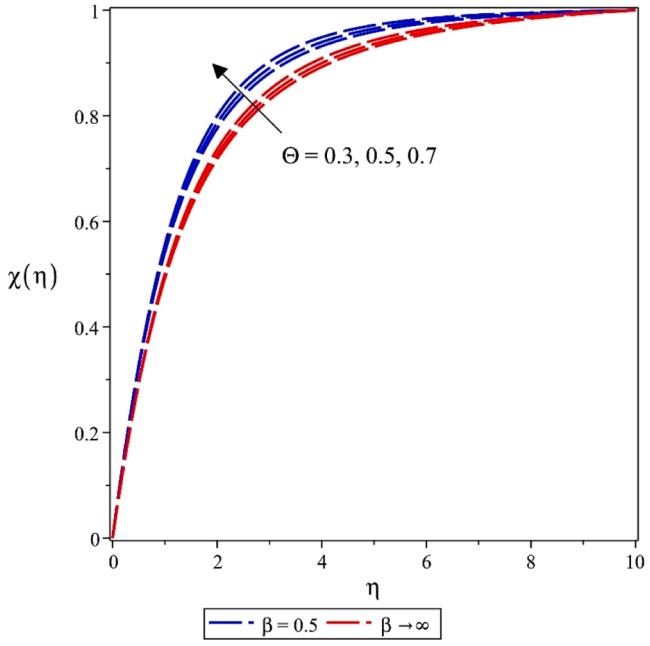


Fig. 9. Impact of Θ on concentration profile $\chi(\eta)$.

Fig. 12. The Nusselt number shows a decreasing nature for both growing values of λ_1 and Θ. Physically, the thermal boundary layer gets thinner upon rising curvature stretching. This leads to low heat transfer at the surface due to heat being distributed over the surface. Also, for larger values of λ_1 indicates slow conduction of heat, thereby reducing the Nusselt number.

The variation in the Sherwood number Sh_s for different values of ζ_1 and Θ are displayed in Fig. 13. It is observed from the figure that Sh_s declined for growing values of both ζ_1 and Θ. Physically, a higher relaxation parameter indicates a slow mass diffusion effect, leading to a delay in the transport of solute particles and a reduced concentration profile. Also, the concentration layer gets thinner due to high diffusion and causes concentration gradients to decline at the surface.

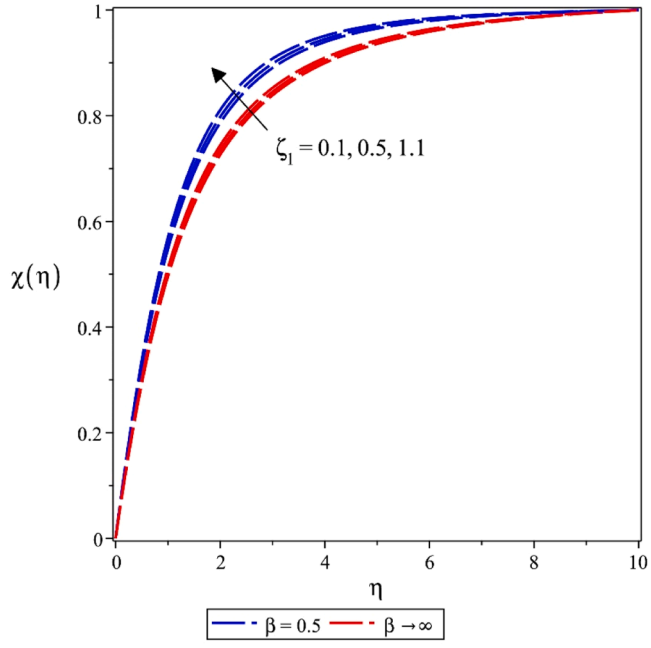


Fig. 10. Effect of ζ_1 over $\chi(\eta)$.

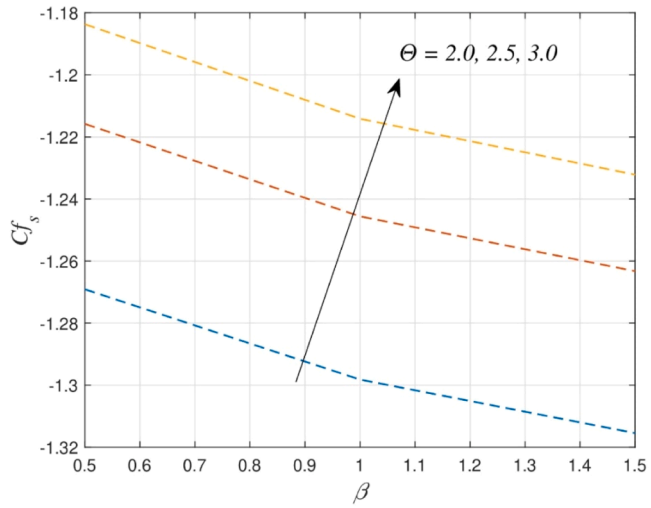


Fig. 11. Nature of Cf_s for varying Θ and β.

The variations observed in all figures of velocity, temperature and concentration profiles showcase the combined influence of various parameters on fluid flow, heat and mass transfer over the bended surface. The increase or decrease of these respective profiles against the parameters illustrates the fluid velocity, heat and mass transfer rates. These responses provide useful insight over many engineering practical processes such as stretching surface, heat and mass transfer management involving coupled fluid velocity, heat and mass transfer phenomena under different physical conditions.

$$Cf_s\% = \left|\frac{Cf_{s_{non-Newtonian\ case}} - Cf_{s_{Newtonian\ case}}}{Cf_{s_{Newtonian\ case}}}\right| \times 100,\ Nu_s\%$$
$$= \left|\frac{Nu_{s_{non-Newtonian\ case}} - Nu_{s_{Newtonian\ case}}}{Nu_{s_{Newtonian\ case}}}\right| \times 100\ Sh_s\%$$
$$= \left|\frac{Sh_{s_{non-Newtonian\ case}} - Sh_{s_{Newtonian\ case}}}{Sh_{s_{Newtonian\ case}}}\right| \times 100$$

Table 3 discusses the quantitative comparison of engineering

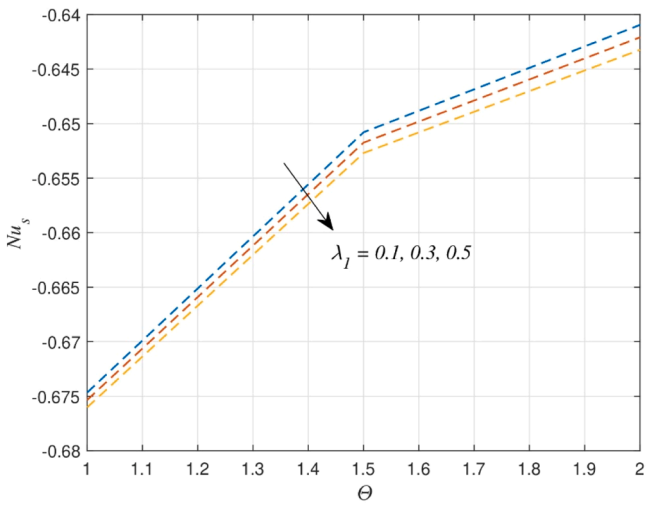


Fig. 12. Nature of the Nu_s for varying λ_1 and Θ.

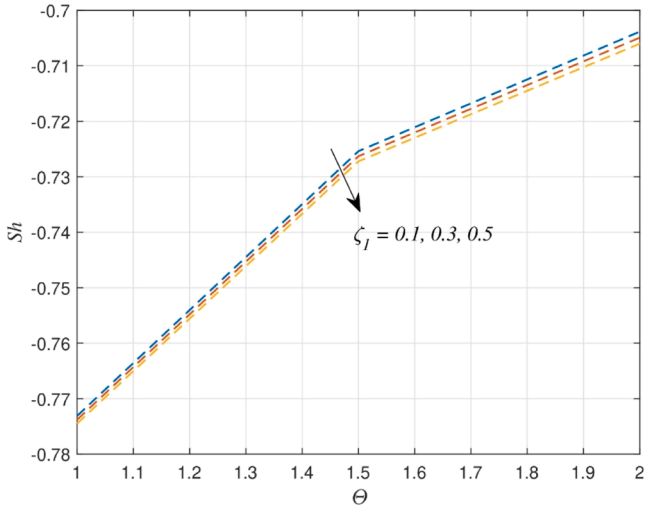


Fig. 13. Nature of the Sh_s for varying values of ζ_1 and Θ.

Table 3
Quantitative analysis of Engineering factors.

α	Θ	λ_1	ζ_1	Cf_s%	Nu_s%	Sh_s%
0.4	0.5	0.3	0.3	3.25	0.91	1.06
0.6	0.5	0.3	0.3	3.89	1.08	1.06
0.8	0.5	0.3	0.3	4.24	1.23	1.06
0.4	0.1	0.3	0.3	0.28	0.04	0.05
0.4	0.3	0.3	0.3	1.57	0.40	0.46
0.4	0.5	0.3	0.3	3.15	0.92	1.08
0.4	0.5	0.5	0.3	3.15	0.99	1.81
0.4	0.5	0.7	0.3	3.15	0.97	1.81
0.4	0.5	0.9	0.3	3.15	0.95	1.81
0.4	0.5	0.3	0.5	3.15	0.92	1.87
0.4	0.5	0.3	0.7	3.15	0.92	1.85
0.4	0.5	0.3	0.9	3.15	0.92	1.83

quantities against several parameters for non-Newtonian and Newtonian case. Cf_s% rises from 3.25 to 4.24 for augmented values of α and rises from 0.28 to 3.15 for increasing values of Θ. But remains constant for different values of thermal and concentration relaxation parameters. Nu_s% has shown an increasing behaviour of 0.91–1.23 and 0.04–0.92 for increasing values of α and Θ parameters respectively. On contrast it declined from 0.99 to 0.95 for increasing values of λ_1 and remained constant for ζ_1. α and λ_1 showed negligible influence on Sh_s% and it if found that Sh_s% increased from 0.05 to 1.08 for growing values of Θ and reduced from 1.87 to 1.83 for ζ_1 parameter.

This quantitative analysis help in analysing comparative impact of governing parameter on friction, heat and mass transfer. The results offer useful insights for better fluid flow and analyse heat and mass transfer rates in thermal control and cooling systems.

5. Conclusion

The present research is focused on the influence of external factors such as variable thermal conductivity and melting effect on Casson fluid dynamics. The Cattaneo-Christov model was used to analyse heat and mass transfer across bended extended surface. A suitable similarity approach was introduced to transform system of PDEs to system of ODEs and numerical solution was obtained using RKF-45th and shooting technique. The parametric analysis was carried out in two different cases which is non-Newtonian and Newtonian case. The important conclusions drawn from this analysis are as follows:

a) The velocity profile falls due to rising values of Casson fluid parameter.
b) Growing values of curvature parameter increases velocity, temperature, and concentration profile.
c) Velocity profile reduces for elevated values of porosity parameter.
d) An augmentation in variable thermal conductivity parameter enhances thermal distribution.
e) Increasing the thermal relaxation parameter decreases the thermal profile but concentration relaxation parameter leads to higher concentration profile.
f) Elevation in curvature parameter and thermal relaxation parameter reduces heat transfer rate.
g) Elevation in concentration relaxation parameter and curvature parameter reduces mass transfer rate.

The current work is limited to steady, boundary layer flow of non-Newtonian fluid over porous curved surface under the effects of melting effect variable thermal conductivity and C-C heat and mass flux model. The numerical solutions were used for theoretical analysis under prearranged assumptions and boundary conditions.

This work can be expanded by considering unsteady flow and 3-D flow over curved sheet with Riga surface under different physical phenomenon like Marangoni effect, exponential heat source/sink and hall current and many more. Analytical or semi analytical methods can be considered for obtaining exact solutions. Further, machine learning, regression, and optimisation techniques can be used to analyse the management of heat and mass transfer rates in many engineering processes. Also, experimental comparison can be incorporated in the future work for applicability of the results in practical applications.

Declaration of Competing Interest

All the authors are hereby declaring that they have no conflict of interest.

Acknowledgements

L.M.P. acknowledges partial financial support from ANID through FONDECYT 1260401 and from the Centers of Excellence with BASAL/ANID CIA250002, CEDENNA.

References

[1] K. Anantha Kumar, V. Sugunamma, N. Sandeep, Effect of thermal radiation on MHD Casson fluid flow over an exponentially stretching curved sheet, J. Thermal Anal. Calorim. 140 (5) (2020) 2377–2385, https://doi.org/10.1007/s10973-019-08977-0.

[2] M. Awais, T. Salahuddin, A. Alalawi, A. Afandi, H. AL Garalleh, Heat and mass transfer in MHD Casson nanofluid with Joule heating and chemical reaction through a Darcy–Forchheimer porous medium, Results Surf. Interfaces 23 (2026) 100795, https://doi.org/10.1016/j.rsurfi.2026.100795.
[3] K. Jat, K. Sharma, P. Choudhary, P. Soni, R. Ali, M. Ganesh, Significance of Darcy–forchheimer Casson fluid flow past a non-permeable curved stretching sheet with the impacts of heat and mass transfer, Case Stud. Thermal Eng. 61 (2024) 104907, https://doi.org/10.1016/j.csite.2024.104907.
[4] M. Saleem, M. Hussain, U. Khan, S.M. Hussain, Comparative analysis of entropy optimization in Casson fluid flow over a nonlinear curved stretching sheet, J. Thermal Anal. Calorim. 150 (12) (2025) 9353–9370, https://doi.org/10.1007/s10973-025-14259-9.
[5] K.M. Nihaal, U.S. Mahabaleshwar, N. Swaminathan, G.V. Bognar, Optimization of heat transfer analysis on an aggregated nanofluid flow over a thin porous needle: sensitivity analysis approach, Int. J. Thermofluids 27 (2025) 101191, https://doi.org/10.1016/j.ijft.2025.101191.
[6] S. Ahmad, S. Nadeem, N. Muhammad, Boundary layer flow over a curved surface imbedded in porous medium, Commun. Theor. Phys. 71 (3) (2019) 344, https://doi.org/10.1088/0253-6102/71/3/344.
[7] M. Mumtaz, S. Islam, H. Ullah, A. Dawar, Z. Shah, A numerical approach to radiative ternary nanofluid flow on curved geometry with porous media and multiple slip constraints, ZAMM - J. Appl. Math. Mech. / Zeitschrift für Angewandte Mathematik und Mechanik 104 (10) (2024) e202300914, https://doi.org/10.1002/zamm.202300914.
[8] N. Ahsan, M.N. Aslam, M.N. Khan, E.A. Az-Zo'bi, Bioconvective flow analysis of non-Newtonian fluid over a porous curved stretching surface, Proc. Inst. Mech. Eng. Part N: J. Nanomater. Nanoeng. Nanosyst. (2024) 23977914241231891, https://doi.org/10.1177/23977914241231891.
[9] B.K. Richa, B.Almohsen Sharma, D. Laroze, Intelligent neuro-computational modelling for MHD nanofluid flow through a curved stretching sheet with entropy optimization: Koo–Kleinstreuer–Li approach, J. Comput. Des. Eng. 11 (5) (2024) 164–183, https://doi.org/10.1093/jcde/qwae078.
[10] N. Ahsan, A. Alhowaity, M.A.H. Abdelmohimen, H.F. Alrihieli, Q.M. Al-Mdallal, Insights of thermal behavior of bioconvective williamson fluid flow over a porous curved stretching surface with chemical reactions: a numerical study, Case Stud. Thermal Eng. 68 (2025) 105924, https://doi.org/10.1016/j.csite.2025.105924.
[11] M.G. Murtaza, E.E. Tzirtzilakis, M. Ferdows, A Note on MHD Flow and Heat Transfer over a Curved Stretching Sheet by Considering Variable Thermal Conductivity 12 (2) (2018).
[12] M. Awais, T. Salahuddin, S. Muhammad, Effects of viscous dissipation and activation energy for the MHD Eyring-powell fluid flow with Darcy-Forchheimer and variable fluid properties, Ain Shams Eng. J. 15 (2) (2024) 102422, https://doi.org/10.1016/j.asej.2023.102422.
[13] K. Ahmed, T. Akbar, I. Ahmed, T. Muhammad, M. Amjad, Mixed convective MHD flow of Williamson fluid over a nonlinear stretching curved surface with variable thermal conductivity and activation energy, Numer. Heat Transf. Part A: Appl. 85 (6) (2024) 942–957, https://doi.org/10.1080/10407782.2023.2194689.
[14] M. Awais, et al., Analysis of Darcy–Forchheimer and variable fluid properties for the flow of Carreau–Yasuda nanofluid over a stretched cylinder with magnetic field effect, Multidiscipl. Model. Mater. Struct. 22 (4) (2026) 1–25, https://doi.org/10.1108/MMMS-10-2025-0414.
[15] S.Z. Alamri, A.A. Khan, I. Nasreen, R. Ellahi, Effect of varying thermal conductivity on MHD micropolar fluid flow based on Cattaneo-Christov heat flux model over an exponentially extended stretching curved surface, JCAMECH 56 (4) (2025), https://doi.org/10.22059/jcamech.2025.398637.1551.
[16] L. Roberts, On the melting of a semi-infinite body of ice placed in a hot stream of air, J. Fluid Mech. 4 (5) (1958) 505–528, https://doi.org/10.1017/S002211205800063X.
[17] Y.-C. Yen, The effect of melting on forced convection heat transfer, J. Appl. Meteorol. (1965), https://doi.org/10.1175/1520-0450(1965)004%3C0523:teomof%3E2.0.co;2.
[18] A.M. Obalalu, A. Darvesh, A.O. Akindele, A. Phulpoto, A.D. Adeshola, M. A. Memon, Analysis of ferrohydrodynamic interaction in unsteady nanofluid flow over a curved stretching sheet with melting heat peripheral conditions, J. Appl. Comput. Mech. 11 (1) (2025) 23–38, https://doi.org/10.22055/jacm.2024.45853.4421.
[19] A. AR, P. Kumar, R. NG, Non-Darcy-Forchheimer flow of Casson-Williamson nanofluid on melting curved stretching sheet influenced by magnetic dipole, ZAMM–J. Appl. Math. Mech./Zeitschrift für Angewandte Mathematik und Mechanik 103 (10) (2023).
[20] R.S. Saif and T. Muhammad, "Melting heat transmission for nanoliquid flow through a curved stretching sheet with Darcy–Forchheimer phenomenon," Waves in Random and Complex Media, pp. 1–21, doi: 10.1080/17455030.2023.2193848.
[21] P. Boonlertnirun, R. Su, A. Sutha, W. Gao, S. Tangaramvong, Mechanics-informed neural network for predicting the axial compressive strength of short circular concrete-filled steel tube columns, Sci. Rep. 16 (1) (2026) 30867, https://doi.org/10.1038/s41598-026-73050-4.
[22] A. Sutha, S. Tangaramvong, T.Z. Win, P. Jongvivatsakul, W. Gao, Physics-informed neural network surrogate and grid-based multi-objective evolutionary optimization for sustainable concrete mix design, Structures 89 (2026) 112120, https://doi.org/10.1016/j.istruc.2026.112120.
[23] S. Nadeem, Z. Ahmed, S. Saleem, Carbon nanotubes effects in magneto nanofluid flow over a curved stretching surface with variable viscosity, Microsyst. Technol. 25 (7) (2019) 2881–2888, https://doi.org/10.1007/s00542-018-4232-4.
[24] P. Ragupathi, N.A. Ahammad, A. Wakif, N.A. Shah, Y. Jeon, Exploration of multiple transfer phenomena within viscous fluid flows over a curved stretching sheet in the co-existence of gyrotactic micro-organisms and tiny particles, Mathematics 10 (21) (2022), https://doi.org/10.3390/math10214133.
[25] B. Nagaraja, K.G. Vidhya, F. Almeida, P. Kumar, Numerical illustration of diffusive flow of blood-based tri-hybrid nanofluid generated by a curved stretching sheet using law of porosity, Numer. Heat Transf. Part A: Appl. 86 (16) (2025) 5626–5647, https://doi.org/10.1080/10407782.2024.2333042.
[26] M. Aldandani, A. Jan, Response surface methodology and sensitivity analysis of RP fluid model over curved stretching sheet: non-similar investigation, Case Stud. Thermal Eng. 68 (2025) 105884, https://doi.org/10.1016/j.csite.2025.105884.
[27] A. Sharma, R.P. Sharma, Statistical and numerical analysis of MHD nanofluid (TiO2/EG) flow on a nonlinear curved stretching surface with heat source: a RSM approach, ZAMM - J. Appl. Math. Mech. / Zeitschrift für Angewandte Mathematik und Mechanik 105 (1) (2025) e202400513, https://doi.org/10.1002/zamm.202400513.
[28] C.M.Z. Umer, I. Ahmad, M.A.Z. Raja, H. Ilyas, K.S. Nisar, M. Shoaib, An intelligent framework for hybrid nanofluid flow over a curved stretching sheet via recurrent neural networks, Soft Comput. (2025), https://doi.org/10.1007/s00500-025-10883-7.
[29] T. Hayat, S. Qayyum, A. Alsaedi, B. Ahmad, Entropy generation minimization: Darcy-Forchheimer nanofluid flow due to curved stretching sheet with partial slip, Int. Commun. Heat Mass Transf. 111 (2020) 104445, https://doi.org/10.1016/j.icheatmasstransfer.2019.104445.